計算数理工学論文集 Vol. 5 (2005 年 6 月), 論文 No. 05-062400 JASCOME

見かけの固有振動数の影響を除いた音場の新しいBEM解析手法 (半無限2次元場での検討)

A NEW BOUNDARY ELEMENT ANALYSIS OF ACOUSTIC FIELDS EXCLUDING INFLUENCE OF FICTITIOUS EIGENFREQUENCIES (STUDY ON 2D HALF-SPACE PROBLEMS)

田中 正隆[1), 松本 敏郎[2), 荒井 雄理[3)

Masataka TANAKA, Toshiro MATSUMOTO, Youri ARAI

1) 信州大学工学部機械システム工学科 (〒 380-8553 長野市若里 4-17-1, E-mail: dtanaka@gipwc.shinshu-u.ac.jp)
2) 名古屋大学大学院工学研究科 (〒 464-8603 名古屋市千種区, E-mail: t.matsumoto@nuem.nagoya-u.ac.jp)
3) 信州大学大学院工学系研究科 (〒 380-8553 長野市若里 4-17-1, E-mail: youri@artist.shinshu-u.ac.jp)

This paper is concerned with a new boundary element method of analysis for 2-dimensional half-space acoustic problems, excluding influence of fictitious eigenfrequencies. It is assumed that the acoustic field is governed by the Helmholtz equation. In solving the external acoustic problem by the usual boundary integral equation, the accuracy of the numerical solution is violated at fictitious eigenfrequencies of the interior problem. The present paper proposes a new boundary element method to circumvent the fictitious eigenfrequency problem by using dual boundary integral equation for nodal points of the boundary element. Through numerical computation of several examples it is demonstrated that the proposed BEM is effective to avoid the fictitious eigenfrequency problem.

Key Words: Computational Mechanics, Boundary Element Method, Dual Boundary Integral Equation, Acoustics, Fictitious Eigenfrequency Problem

1. はじめに

Helmholtz 方程式に支配される音場の問題において，境界積分方程式を用いて外部境界値問題を解く際に重要となるのは見かけの固有振動数問題の影響をいかに回避して精度の良い解を得るかである．見かけの固有振動数問題は，境界積分方程式を用いて無限領域 Ω を含む外部境界値問題を解く際に，解析する振動数が別の内部問題の固有振動数に一致する場合，本来補領域 $\bar{\Omega}$ で音圧が 0 でなければならないのが 0 とならず考察領域 Ω に影響を及ぼし解の精度を著しく乱す問題である [3]．

見かけの固有振動数問題を回避する簡便な手法として知られているのは，補領域 $\bar{\Omega}$ に点（外点）を配置して最終的な方程式系を最小二乗法で解く方法である [9]．この手法は外点を配置する場所やその個数などの考察を必要とし，点の配置の仕方によっては見かけの固有振動数問題を回避できないという欠点を有している．他の方法として代表的なのは，通常の境界積分方程式 (OBIE) とそれを微分した導関数境界積分方程式 (DBIE) を線形結合した式を境界積分方程式として用いる Burton - Miller 法である [10]．ただし，この手法は結合係数を適切に決定しないと見かけの固有振動数の問題を回避できないという欠点を有する．

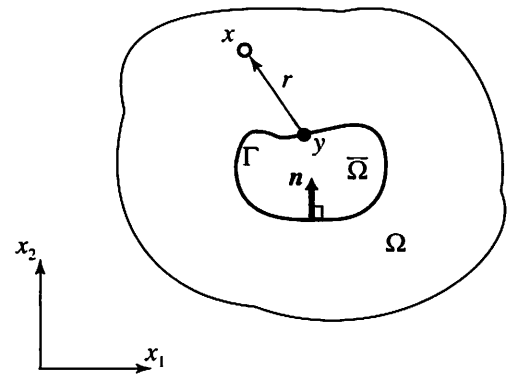

Fig. 1 External problem

本論文で提案する手法は，境界積分方程式（OBIE）とその導関数境界積分方程式（DBIE）をソース点 y の位置により使い分ける方法である．本手法は，OBIE と DBIE で見かけの固有振動数が生じる周波数が異なること [10] を利用して，解くべき方程式系の見かけの固有振動数問題を回避するものである．本手法によれば，外点の配置に関する考察や積分方程式を結合する際の係数の決定に関する考察を必要とせずに問題を回避できるため，音場の最適設計を行う際に極めて有効な手法であるいえる．

2. 理論

本研究で取り扱う外部問題を境界積分方程式を用いて解く場合には，対応する内部問題の固有振動数に等しい周波数で系方程式が不定となり，物理的に意味の無い解が得られてしまう．この問題の原因は，外部問題に対する積分方程式が内部問題の積分方程式と同じ形になることより生じる．そこで本研究では，この問題を回避するため境界積分方程式の導関数を併用する．導関数境界積分方程式を用いて外部境界値問題を解いた際にも同様に見かけの固有振動数問題の影響を受ける．しかしながら，2 つの境界積分方程式においてそれぞれ対応する固有値は異なる．本研究では，同じ問題に対して境界積分方程式とその導関数の境界積分方程式を準備し，それらの式を連立させることで外部問題を解く際の最終的な代数方程式が内部問題の代数方程式と異なるようにして見かけの固有振動数問題を回避する．以下に本研究で用いる境界積分方程式とその導関数境界積分方程式の定式化について記述する．

2.1. 境界積分方程式

音場の支配微分方程式が以下の Helmholtz 方程式で与えられる音響問題に対する境界要素法による定式化について簡単に説明する．

$$\nabla^2 p(x) + k^2 p(x) + f(x) = 0 \tag{1}$$

ここで，$p(x)$ は音圧，$f(x)$ は内部音場の集中音源等を表すソース項である．また，k は波数であり c を音速とすれば次式で表される．

$$k = \frac{\omega}{c} \tag{2}$$

境界要素法による定式化は支配微分方程式 (1) に対して基本解 $p^*(x,y)$ をかけ，考察領域全体で積分した以下の恒等式を出発点とする．

$$\int_\Omega \left\{\nabla^2 p(x) + k^2 p(x) + f(x)\right\} p^*(x,y)\, d\Omega = 0 \tag{3}$$

定式化の際に必要となる基本解 $p^*(x,y)$ とその外向き法線方向微分 $q^*(x,y)$，Laplace 方程式の基本解の外向き法線方向微分 $Q^*(x,y)$ はそれぞれ 2 次元問題の場合次式となる．

$$p^*(x,y) = -\frac{\mathrm{i}}{4} H_0^{(2)}(kr) \tag{4}$$

$$q^*(x,y) = \frac{\partial p^*(x,y)}{\partial n} = \frac{\mathrm{i}}{4} k H_1^{(2)}(kr) \frac{\partial r}{\partial n}(x) \tag{5}$$

$$Q^*(x,y) = -\frac{1}{2\pi r} \frac{\partial r}{\partial n}(x) \tag{6}$$

なお，上式における $H_0^{(2)}$ と $H_1^{(2)}$ はそれぞれ 0 次と 1 次の第 2 種 Hankel 関数である．式 (3) に対して部分積分を 2 回行い，Dirac デルタ関数の性質を考慮し，一様ポテンシャル条件により正則化することで以下の境界積分方程式が導出される [1][5]．ただし，式 (1) において関数 $f(x)$ は集中音源と仮定した．

$$\begin{aligned}&\int_\Gamma \{q^*(x,y) - Q^*(x,y)\} p(x)\, d\Gamma(x) \\ &\quad + \int_\Gamma Q^*(x,y) \{p(x) - p(y)\}\, d\Gamma(x) \\ &\quad = -\mathrm{i}\omega\rho \int_\Gamma p^*(x,y)\, v(x) d\Gamma(x) + I p^*(x^s, y)\end{aligned} \tag{7}$$

式 (7) において x^s は集中音源の座標であり，I は集中音源の強さを表している．また，$v(x)$ は粒子速度である．

正則化された境界積分方程式 (7) は基本解 $Q^*(x,y)$ の特異性が 1 階低減されているため，2 次元問題の場合は全ての積分を直接数値的に評価することが可能である．通常の音響問題では，境界積分方程式 (7) を境界要素で離散化して音圧 p と粒子速度 v に関する代数方程式を求め，この方程式系に境界条件を適用して解けばよい．

2.2. 導関数境界積分方程式

本研究で用いる導関数境界積分方程式は，正則化された境界積分方程式 (7) をソース点 y で微分し，音圧の勾配が一様である場を考えて正則化した式である [6]．以下にその導出手順を示すが，説明の簡素化のため集中音源に関する項は途中の式において省略されていることに注意されたい．

境界積分方程式 (7) をソース点 y で微分することで次式を得る．

$$\begin{aligned}&\int_\Gamma \left\{q^*_{,j}(x,y) - Q^*_{,j}(x,y)\right\} p(x)\, d\Gamma(x) \\ &\quad + \int_\Gamma Q^*_{,j}(x,y) \{p(x) - p(y)\}\, d\Gamma(x) \\ &\quad - \left\{\int_\Gamma Q^*(x,y)\, d\Gamma(x)\right\} p_{,j}(y) \\ &\quad = -\mathrm{i}\omega\rho \int_\Gamma p^*_{,j}(x,y)\, v(x) d\Gamma(x)\end{aligned} \tag{8}$$

ここで，基本解の微分 $p^*_{,j}(x,y)$ は以下のように正則な部分と特異な部分に分けることができる [5]．

$$p^*_{,j}(x,y) = p^*_{R,j}(x,y) + u^*_{,j}(x,y) \tag{9}$$

ここで，$p^*_{R,j}(x,y)$ は正則な項であり，$u^*_{,j}(x,y)$ は Laplace の基本解の微分であり特異性を有する項である．また，式 (8) の左辺第 3 項はソース点 y の位置により決まる定数 $c(y)$ との関係があり，それと式 (9) を考慮することで式 (8) は以下のようになる．

$$\begin{aligned}C_{ij}(y)\, p_{,i}(y) &+ \int_\Gamma \left\{q^*_{,j}(x,y) - Q^*_{,j}(x,y)\right\} p(x)\, d\Gamma(x) \\ &+ \int_\Gamma Q^*_{,j}(x,y) \{p(x) - p(y)\}\, d\Gamma(x) \\ &= -\mathrm{i}\omega\rho \int_\Gamma \left\{p^*_{,j}(x,y) - u^*_{,j}(x,y)\right\} v(x) d\Gamma(x) \\ &\quad - \mathrm{i}\omega\rho \int_\Gamma u^*_{,j}(x,y)\, v(x)\, d\Gamma(x)\end{aligned} \tag{10}$$

式 (10) において基本解 $u^*_{,j}(x,y)$ および $Q^*_{,j}(x,y)$ は 2 次元問題の場合，それぞれ強い特異性 $O(1/r)$ と超特異性 $O(1/r^2)$ を有している．そこで，積分を直接数値的に評価できるようにするために，音圧の勾配が一様である場を考えて正則化を行う [6]．一様な音圧勾配の場において $p(x)$ および $q(x)$ はそれぞれ以下のようになる．

$$p(x) = p(y) + r_m(x,y)\, p_{,m}(y) \tag{11}$$

$$q(x) = n_m(x)\, p_{,m}(y) \tag{12}$$

式 (11)，(12) を Laplace 方程式の正則化された境界積分方程式を微分した関係式 [7] に代入すれば，次の積分方程式を得る．

$$\begin{aligned} &C_{ij}(y)\, p_{,i}(y) + \int_\Gamma Q^*_{,j}(x,y)\, r_m(x,y)\, p_{,m}(y)\, d\Gamma(x) \\ &\quad = \int_\Gamma u^*_{,j}(x,y)\, n_m(x)\, p_{,m}(y)\, d\Gamma(x) \end{aligned} \tag{13}$$

式 (10) から式 (13) を差し引き，両辺に $n_j(y)$ を乗じ，これまで省略していた集中音源に関する項を追加すれば，以下の正則化された導関数積分方程式を得る．

$$\begin{aligned} &\int_\Gamma \left\{\tilde{q}^*(x,y) - \tilde{Q}^*(x,y)\right\} p(x)\, d\Gamma(x) \\ &+ \int_\Gamma \tilde{Q}^*(x,y)\left\{p(x) - p(y) - r_m(x,y)\, p_{,m}(y)\right\} d\Gamma(x) \\ &= -\mathrm{i}\omega\rho \int_\Gamma \left\{\tilde{p}^*(x,y) - \tilde{u}^*(x,y)\right\} v(x) d\Gamma(x) \\ &-\mathrm{i}\omega\rho \int_\Gamma \tilde{u}^*(x,y)\left\{v(x) - n_m(x)\, p_{,m}(y)\right\} d\Gamma(x) \\ &\quad + I\tilde{p}^*(x^s,y) \end{aligned} \tag{14}$$

ただし，$\tilde{()} = \frac{\partial()}{\partial y_j} n_j(y)$ であり，基本解は 2 次元問題の場合それぞれ以下のように与えられる．

$$\tilde{u}^*(x,y) = -\frac{1}{2\pi r}\frac{\partial r}{\partial n}(y) \tag{15}$$

$$\tilde{Q}^*(x,y) = \frac{1}{2\pi r^2}\left\{2\frac{\partial r}{\partial n}(x)\frac{\partial r}{\partial n}(y) + n_j(x)\, n_j(y)\right\} \tag{16}$$

$$\tilde{p}^*(x,y) = \frac{\mathrm{i}}{4} k H_1^{(2)}(kr)\frac{\partial r}{\partial n}(y) \tag{17}$$

$$\begin{aligned} \tilde{q}^*(x,y) = \frac{\mathrm{i}}{4}k\Bigg[&kH_0^{(2)}(kr)\frac{\partial r}{\partial n}(x)\frac{\partial r}{\partial n}(y) \\ &-H_1^{(2)}(kr)\frac{1}{r}\left\{n_j(x)\, n_j(y) + 2\frac{\partial r}{\partial n}(x)\frac{\partial r}{\partial n}(y)\right\}\Bigg] \end{aligned} \tag{18}$$

式 (14) において $\tilde{u}^*(x,y)$ については 1 階，$\tilde{Q}^*(x,y)$ については 2 階それぞれ特異性がキャンセルされているため全ての積分を数値的に直接評価可能である．しかし，特異性がキャンセルされている場合でも，数値積分区間内の内部にソース点が置かれることは精度上好ましくない．そこで本研究では，内挿関数の性質を利用して積分の数値的評価を行う場合にも特異性がキャンセルされている形を採用した [8]．

以上導出された 2 つの境界積分方程式を併用して見かけの固有振動数問題を回避する．

3. 数値解析

3.1. 解析例題 1

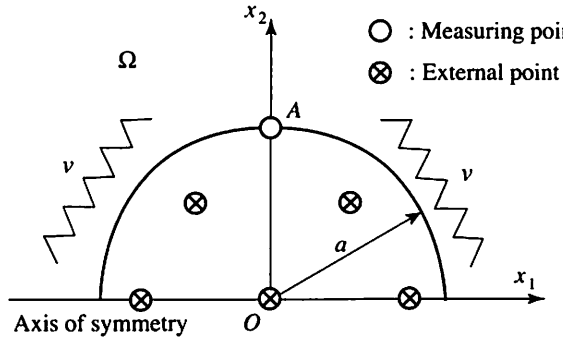

Fig. 2　Analysis model 1

本手法の有効性を確かめるために，解析解が得られる半無限空間に表面が一様に振動している呼吸円筒が存在する場合を考える（図 2）．境界は 2 次のアイソパラメトリック要素を用いて離散化を行った．その場合ソース点 y が要素の中間節点に一致する場合に導関数境界積分方程式 (14) を用い，ソース点が要素端の節点に一致する場合は通常の境界積分方程式 (7) を用いる（図 3）．媒質密度 $\rho = 1.2\,[\mathrm{kg/m^3}]$，伝播速度 $c = 340\,[\mathrm{m/s}]$，呼吸円筒の半径 $a = 0.2\,[\mathrm{m}]$ とした．呼吸円筒の表面は $v = 1.0\,[\mathrm{m/s}]$ の境界条件を与え，円筒表面を一様に境界要素分割するとし，全要素数は 192 とした．また，解析対象が x_1 軸に関して対称であるため対称性を考慮した基本解を用いることとした [2]．2 次元無限平面内で振動する呼吸円筒の解析解は次式で与えられる [16]．

$$p(r) = -\mathrm{i}v\rho c\frac{H_0^{(2)}(kr)}{H_1^{(2)}(ka)} \tag{19}$$

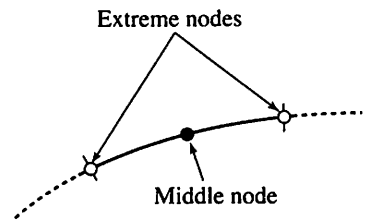

Fig. 3　Boundary element

数値解析で得られた境界表面上の点 A での音圧を音圧レベルに変換したものをプロットする．

図 4 に，通常の境界積分方程式 (7) を用いて得られる計算結果を解析解と比較して示す．$ka = 5.2$ 付近で見かけの固有振動数の影響により正確な結果が得られていないことが分かる．

図 5 に解析解と提案手法を比較した結果を示す．本手法がいずれの周波数でも見かけの固有振動数の影響を回避し，解析解に良く一致する結果が得られていることが分かる．図 5 は，ソース点 y が要素を構成する中間節点に位置した場合に導関数境界積分方程式 (14) を適用した結果である．

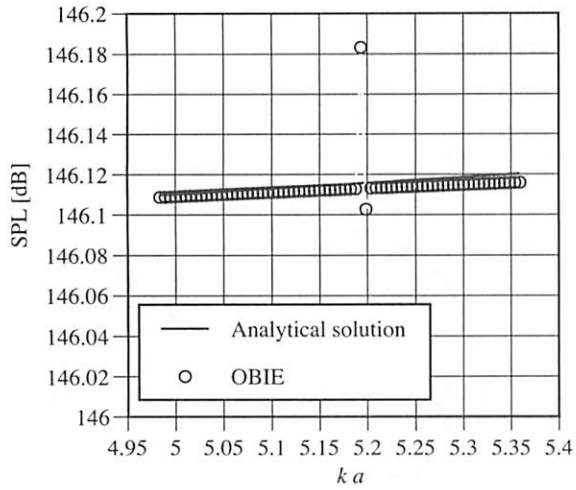

Fig. 4　Numerical results 1

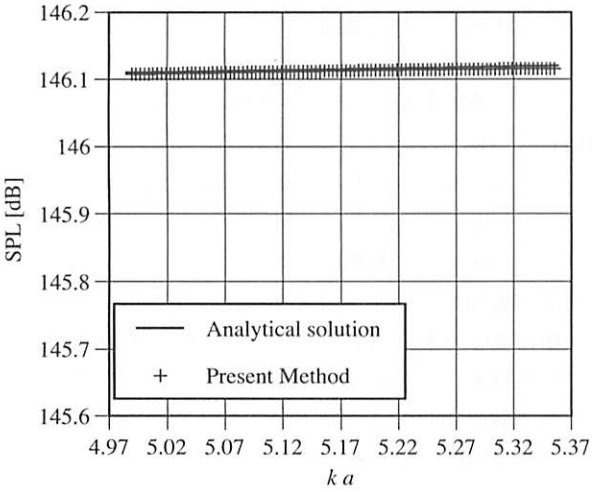

Fig. 5　Numerical results 2

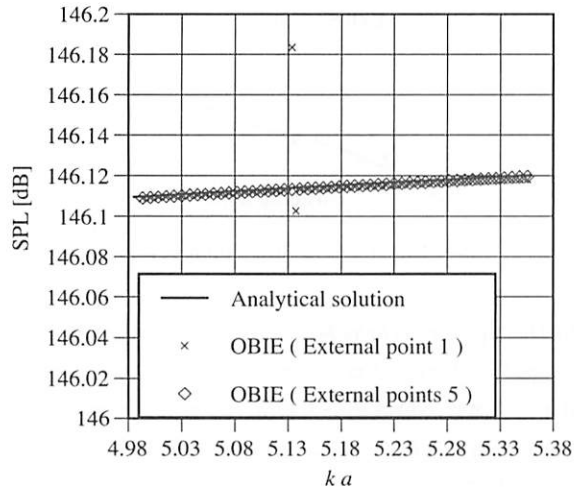

Fig. 6　Numerical results 3

図 6 は，解析解と外点を配置して見かけの固有振動数を回避する手法を比較したものを示す．外点の配置は，原点に 1 点のみ配置した場合と図 2 に示す 5 点全てを使用した場合の 2 通りに関して解析を行った．数値解析結果より，外点を 1 点配置するだけでは全く効果がないことがわかり，5 点配置しないと問題を回避できないことがわかる．このことより本手法の方が，外点の配置に関する考察を必要しないため非常に効率的であるといえる．

3.2. 解析例題 2

解析対象として図 7 に示すように，半無限空間内に直壁が存在する場合を考える．媒質密度 $\rho = 1.2[\mathrm{kg/m^3}]$，伝播速度 $c = 340[\mathrm{m/s}]$，点音源 A の強さを $(2.0, 0.0)[\mathrm{Pa}]$ として与えた．周波数は 150[Hz] から 250[Hz] を 1[Hz] 刻みにとって解析を行う．評価点は地表面に 1 点設置し，この点で得られる音圧を音圧レベルに変換したものをプロットする．ここで，x_1 軸は完全反射とするためそれを考慮し対称性の基本解を用いるものとし，対称軸上の要素分割は不要となる．数値解析するにあたって直壁表面を境界 2 次要素を用い，全要素数 310 で離散化し，直壁の境界条件は完全反射の条件を与えた．

この問題に対する解析解を求めるのは非常に困難なため，直壁の内側にさらに境界がある 3 重連結領域を考え，その境界に完全反射の境界条件を与えた．そのため，直壁を通過してくる音波がそこで反射して考察領域に影響が及ばない．なお，内側の境界は境界 2 次要素を用い，全要素数 90 で離散化を行った．

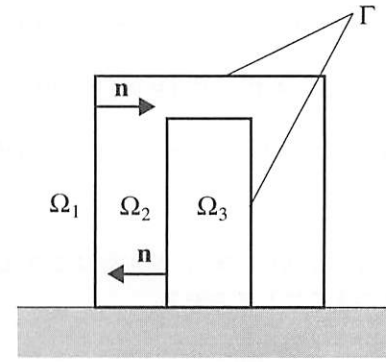

Fig. 8　Multiply connected domain

図 9 に通常の境界積分方程式 (7) と 3 重連結領域を考えて解析した結果を比較して示す．周波数 200[Hz] 付近において見かけの固有振動数の影響により解の精度が落ちていることがわかる．

図 10 は提案手法と 3 重連結領域を考えて解析したものを比較した結果を示している．本手法がいずれの周波数でも見かけの固有振動数の影響を回避し，解析解に良く一致する結果が得られていることが分かる．図 10 は，ソース点 y が要素を構成する中間節点に位置した場合に導関数境界積分方程式 (14) を適用し，要素の端の節点では通常の境界積分方程式 (7) を適用した結果である．

図 11 には，外点を配置して見かけの固有振動数を回避する手法と 3 重連結領域を考えて解析し，それらを比較したものを示す．外点の配置は，図 12 に示すように直壁の中心に 1 点のみ配置した．数値解析結果より，外点を 1 点付加した場合，通常の境界積分方程式 (11) を用いた場合より精度が

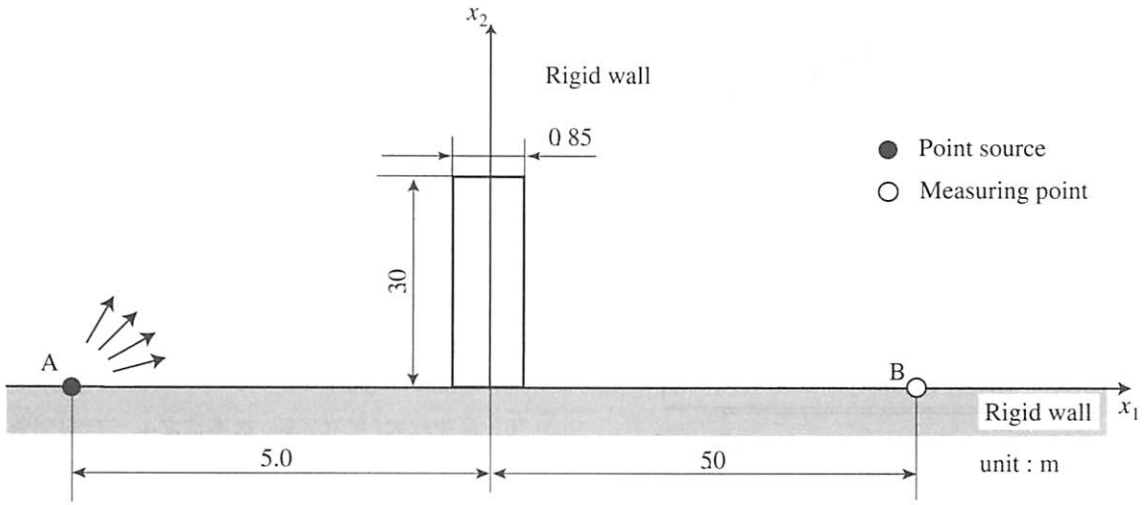

Fig. 7　Analysis model 2

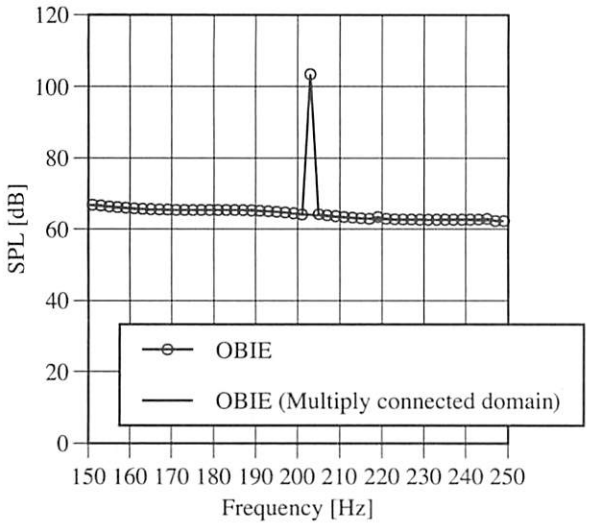

Fig. 9　Numerical results 4

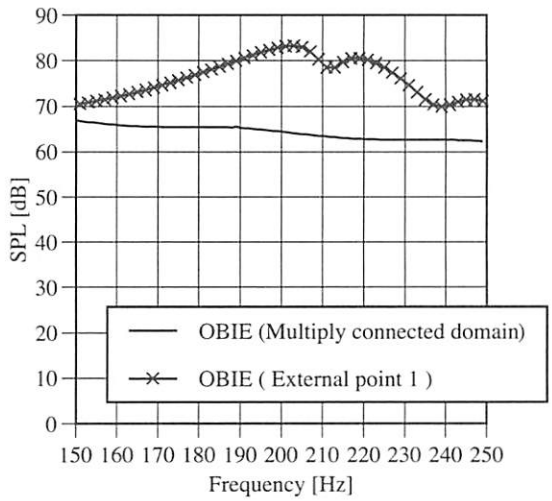

Fig. 11　Numerical results 6

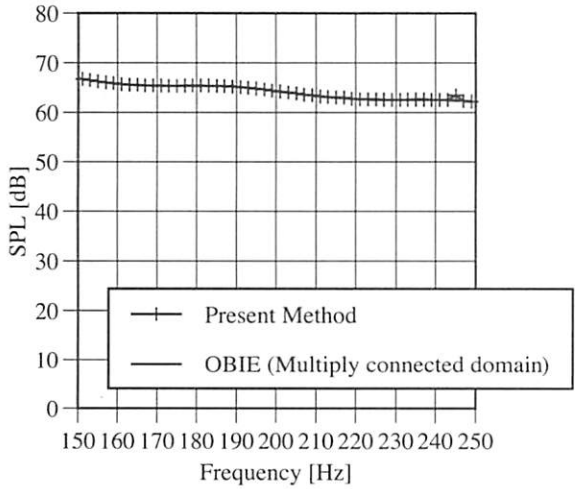

Fig. 10　Numerical results 5

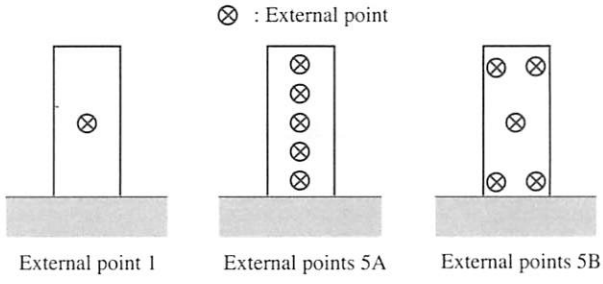

Fig. 12　Location of external point

極端に落ちていることが確認できる．

そこで，図 12 に示すように異なる配置で外点を 5 点用いて解析した結果を図 13 に示す．異なる 5 点の配置で解析を行った場合も解の精度も極端に悪いことが確認できる．

以上，外点を付加して解析した場合の結果より，外点を付

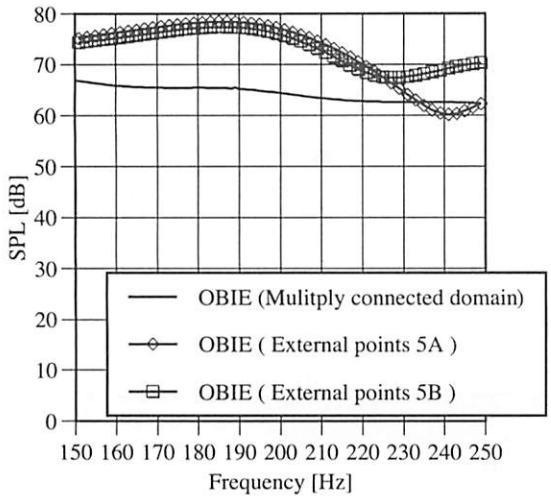

Fig. 13　Numerical results 7

加して見かけの固有振動数問題を回避するのは問題によっては非常に困難になる可能性があることがわかる．そのため本手法の方がこの問題を回避するための手法として効果的であることが確認された．

4. 結言

Helmholtz 方程式に支配される 2 次元定常音響問題を解析する際に重要となる見かけの固有振動数問題を回避する新しい境界要素解析手法を提案した．本手法の有効性を確認するため，解析解が求められる呼吸円筒の問題および半無限空間内に直壁が存在する問題を取り上げ，その問題を提案手法に基づく解析プログラムで数値解析を行い，精度のよい解が得られることを確認した．本手法では，外点の配置に関する考察が必要ではなく，見かけの固有振動数問題を効率的に回避することが可能である．本手法は，音場の最適形状設計などのように反復計算ごとに形状が変化する問題などに非常に有効であると考えられるため，そのような問題に対して適用する予定である．

本報では 2 次元問題に限定して理論を展開しているが，3 次元問題に拡張した場合においても見かけの固有振動数問題を効率的に回避可能である．

参考文献

(1) 田中正隆, 松本敏郎, 中村正行：境界要素法， 培風館, (1991).

(2) 榎園正人：境界要素解析, 培風館, (1986).

(3) 小林昭一：波動解析と境界要素法, 京都大学学術出版会, (2000).

(4) 田中正隆, 荒井雄理 （共訳）; J.T. Katsikadelis（著）：境界要素法ー基本と応用ー, 朝倉書店, (2004).

(5) 松本敏郎, 田中正隆: 正則化された境界積分方程式の離散化手法, BEM・テクノロジー・コンファレンス論文集, **1** (1991), pp.7–12.

(6) 荒井政大, 足立忠晴, 松本浩之：一様勾配条件に基づく境界要素解析の高精度化（ポテンシャル問題に対する定式化への適用）, 日本機械学会論文集 (A 編), **61**-581 (1995), pp.161–168.

(7) 松本敏郎, 田中正隆, 岡山瞬： 二次元ポテンシャル問題における超特異積分方程式と正則化された境界積分方程式による境界のポテンシャル勾配の評価法, 日本機械学会論文集 (A 編), **64**-619 (1998), pp.743–750.

(8) Matsumoto, T., Tanaka, M., Sladek. V, and Sladek ,J. (eds.) : *Singular Integrals in Boundary Element Methods*, Computational Mechanics Pulications, pp.263–297 (2002).

(9) H. A.Schench：Improved integral formulation for acoustic radiation problems, *J. Acoust. Soc. Am.*, **44**-1 (1968), pp.45–58.

(10) A. J. Burton, and G. F. Miller： The application of integral equation methods to the numerical solution of some exterior boundary-value problems, *Proc. Roy. Soc. London, Ser. A*, **323** (1971), pp.201–210.

(11) 一宮亮一：機械系の音響工学， コロナ社, (1992).

(12) 小橋豊：音と音波， 裳華房, (1968).

(13) 日本音響学会（編）：騒音・振動， コロナ社, (1982).

(14) 早坂寿雄：技術者のための音響工学， 丸善株式会社, (1986).

(15) 日本音響学会 （編）：基礎音響工学, コロナ社, (1990).

(16) 三井田惇郎：音響工学, 昭晃堂, (1987).

Transactions of JASCOME, Vol. 5 (June 2005), Paper No. 05-062401 JASCOME

ACCELERATING MULTI-DOMAIN HYBRID BOUNDARY NODE METHOD WITH FAST MULTIPOLE METHOD

Jianming ZHANG [1], Masataka TANAKA [2], Morinobu ENDO [3]

1) Faculty of Engineering, Shinshu University, (Nagano 380-8553, e-mail: zhangjm@homer.shinshu-u.ac.jp)

2) Faculty of Engineering, Shinshu University, (Nagano 380-8553, e-mail: dtanaka@gipwc.shinshu-u.ac.jp)

3) Faculty of Engineering, Shinshu University, (Nagano 380-8553, e-mail: endo@endomoribu.shinshu-u.ac.jp)

This work presents a fast implementation of the multi-domain hybrid boundary node method (HdBNM) for numerical solution of Laplace's equation. The preconditioned GMRES is employed to solve the overall system of equations. At each iteration step of the GMRES, the matrix-vector multiplication is split into smaller scale ones at the subdomain level, and accelerated by the fast multipole method independently within individual subdomains. The computed matrix-vector products at the subdomain level are then assembled into an overall vector using the equilibrium and continuity conditions at the interfaces. Our method is tested by two benchmark examples for three-dimensional potential problems, and high accuracy and efficiency are observed.

Keywords: meshless method; hybrid boundary node method; multi-domain formulation; fast multipole method

1. Introduction

Meshless techniques to obtain numerical solutions for PDEs without resorting to an element frame have been popular throughout the computational mechanics community for the past two decades. This is because, with mesh-based techniques such as the finite element method (FEM) or the boundary element method (BEM), the task of mesh generation for complex geometries is often time-consuming and prone to errors, and the difficulties with re-meshing in problems involving moving boundaries, large deformations or crack propagation are crucial. Many meshless methods have been proposed so far. Some of the methods are the element free Galerkin method (EFG) [1], the meshless local Petrov-Galerkin (MLPG) approach [2], the boundary node method (BNM) [3] and the hybrid boundary node method (HdBNM) [4-6]. Among these methods, the HdBNM is a truly meshless boundary-only method, which combines the MLS approximation scheme with the hybrid displacement variational formulation. It not only has the advantage of reducing the spatial dimensions by one as BEM, but also does not require any cells either for interpolation of the solution variables or for the boundary integration. In fact, the HdBNM requires only discrete nodes located on the surface of the domain and its parametric representation. As the parametric representation of created geometry is used in most of CAD packages, it should be possible to exploit their *Open Architecture* features, and automatically obtain required coefficients (representation).

However, like in the traditional BEM, the system matrix of the HdBNM is dense and unsymmetrical. The computational time and memory requirement for directly factoring such system increase respectively with $O(N^3)$ and $O(N^2)$, where N is the total number of degrees of freedom. In order to obtain an efficient algorithm not only in terms of human-labor costs (where mesh generation is avoided) but also in terms of computer costs, we have recently combined the HdBNM with the fast multipole method (FMM) [7-10]. The combined approach (here called FM-HdBNM) reduces both the memory requirement and the total execution count to $O(N)$. Therefore, it is promising for large scale computations. In this paper, we further implement the FMM techniques in a multi-domain formulation of the HdBNM.

Multi-domain formulations are employed when the entire domain under consideration is governed by individual differential equations in different parts and/or constructed of different materials. Besides, in the case of a domain with complicated boundary profile or parallel computation, the domain may be decomposed for better computational efficiency. In a multi-domain solver, the original domain is divided into a finite number of sub-domains, and in each of them the full integral representation formula is applied. At the common interfaces between the adjacent subdomains, the corresponding full matching conditions are enforced. How to satisfy the continuity and equilibrium conditions at the interfaces is one of the important aspects of implementation for a multi-domain algorithm. There are mainly two methods in the literature: the standard multi-domain method [11] and the domain decomposition method [12]. In the standard multi-domain method, the discretized equations corresponding to the subdomains are assembled into a system of equations according the boundary and interface conditions. While the matrices that arise in the single domain formulation are fully populated, the multi-domain formulation leads to overall matrix equations with a sparse blocked structure. In the domain decomposition method, the interface conditions are assumed and then the subdomain problems are solved independently. The modification of the interface condition is usually iterative

using different methodologies, as the Schwarz Neumann-Neumann and Schwarz Dirichlet-Neumann methods. Repetition of the iteration process is continued until convergence. The domain decomposition method allows different type of discretization methods (e.g. BEM and FEM) to be used for a numerical solution of the individual subdomains and coupling between them without accessing to the source codes of the methods. However, it has some relevant parameters to be chosen and the optimal values for these parameters are usually problem-dependent. This arbitrariness represents a disadvantage of the method. In the present paper, we adopt the standard multi-domain method, and make full use of the resultant sparsity of the matrix equations during the solution process. As the sparse structure of the matrix is directly related to the ordering of blocks occurring in the matrix, we use the ordering strategy suggested by Kane [11] to obtain an optimal blocks structure. The preconditioned restarted GMRES is employed to solve the system equations. At each step of the iterations of GMRES, the matrix-vector multiplication is accelerated by the FMM at the subdomain level. Therefore, the FM-HdBNM code for single domain problem can be used directly. The algorithm is implemented through a code written in C++. In the code, an interface class is devised to deal with the equilibrium and continuity conditions at the interfaces. Two benchmark examples of three-dimensional potential problems are investigated. Numerical results demonstrate the accuracy and efficiency of the proposed approach.

2. Multi-domain formulation of HdBNM

In this section, we will derive a multi-domain formulation for solving 3D potential problems. The formulation is obtained by assembling the equations for each single domain into an overall system of equations using the continuity and equilibrium relations along the interfaces between the subdomains. The HdBNM formulation for solving single domain problems has been given in reference [5]. For the sake of simplicity and to allow for a clear presentation of the multi-domain formulation, we consider here three subdomains.

The hybrid boundary node method is based on a modified variational principle, in which there are three independent variables, namely:

- temperature within the domain, ϕ ;
- boundary temperature, $\tilde{\phi}$;
- boundary normal heat flux, $\tilde{q}$.

Suppose further that N nodes are randomly distributed on the bounding surface of subdomain-1. The temperature within the domain is approximated using fundamental solutions as follows:

$$\phi = \sum_{I=1}^{N} \phi_I^s x_I \tag{1}$$

and hence at a boundary point, the normal flux is given by

$$q = -\kappa_1 \sum_{I=1}^{N} \frac{\partial \phi_I^s}{\partial n} x_I \tag{2}$$

where ϕ_I^s is the fundamental solution with the source at a node $\mathbf{s}_I$; κ_1 is the heat conductivity and x_I are unknown parameters. For 3-D potential problems, the fundamental solution can be written as

$$\phi_I^s = \frac{1}{\kappa_1} \frac{1}{4\pi r(Q, \mathbf{s}_I)} \tag{3}$$

where Q is a field point; $r(Q, \mathbf{s}_I)$ is the distance between Q and $\mathbf{s}_I$.

The boundary temperature and normal heat flux are interpolated by moving least square (MLS) approximation [5]:

$$\tilde{\phi}(\mathbf{s}) = \sum_{I=1}^{N} \Phi_I(\mathbf{s}) \hat{\phi}_I \tag{4}$$

$$\tilde{q}(\mathbf{s}) = \sum_{I=1}^{N} \Phi_I(\mathbf{s}) \hat{q}_I \tag{5}$$

In the foregoing equations, $\Phi_I(\mathbf{s})$ is the shape function of MLS approximation; $\hat{\phi}_I$ and $\hat{q}_I$ are nodal values of temperature and normal flux, respectively.

Using the modified functional variational principle in all local-regions around the boundary nodes, the following set of HdBNM equations can be written for subdomain-1:

$$\mathbf{U}\mathbf{x} = \mathbf{H}\hat{\boldsymbol{\phi}} \tag{6}$$

$$\mathbf{Q}\mathbf{x} = \mathbf{H}\hat{\mathbf{q}} \tag{7}$$

In the above equations, the elements of matrices **U**, **Q** and **H** are given by

$$U_{JI} = \int_{\Gamma_{s_J}} \phi_I^s(Q, \mathbf{s}_I) v_J(Q) d\Gamma \tag{8}$$

$$Q_{JI} = \int_{\Gamma_{s_J}} \frac{\partial \phi_I^s(Q, \mathbf{s}_I)}{\partial n(Q)} v_J(Q) d\Gamma \tag{9}$$

$$H_{JI} = \int_{\Gamma_{s_J}} \Phi_I(Q) v_J(Q) d\Gamma \tag{10}$$

where v_J is a weight function and $\mathbf{s}_I$ is a boundary point, Γ_{s_J} is a regularly shaped local region around a given node $\mathbf{s}_J$ in the parametric representation space of the boundary surface. (For full details of HdBNM refer to [5]).

To assemble equations (5) and (6) into an overall system of equation for the entire domain later, we sort the boundary nodes into three groups: group 1 containing nodes that belong exclusively in subdomain-1, group 2 containing nodes that are on the interface with subdomain-2, and group 3 containing nodes on the interface with subdomain-3. Correspondingly, equations (5) and (6) are partitioned into blocked matrix equations as

$$\begin{bmatrix} U_{11}^1 & U_{12}^1 & U_{13}^1 \\ U_{21}^1 & U_{22}^1 & U_{23}^1 \\ U_{31}^1 & U_{32}^1 & U_{33}^1 \end{bmatrix} \begin{Bmatrix} x_1^1 \\ x_2^1 \\ x_3^1 \end{Bmatrix} = \begin{Bmatrix} H_1^1 \hat{\phi}_1^1 \\ H_2^1 \hat{\phi}_2^1 \\ H_3^1 \hat{\phi}_3^1 \end{Bmatrix} \tag{11}$$

$$\begin{bmatrix} Q_{11}^1 & Q_{12}^1 & Q_{13}^1 \\ Q_{21}^1 & Q_{22}^1 & Q_{23}^1 \\ Q_{31}^1 & Q_{32}^1 & Q_{33}^1 \end{bmatrix} \begin{Bmatrix} x_1^1 \\ x_2^1 \\ x_3^1 \end{Bmatrix} = \begin{Bmatrix} H_1^1 \hat{q}_1^1 \\ H_2^1 \hat{q}_2^1 \\ H_3^1 \hat{q}_3^1 \end{Bmatrix} \tag{12}$$

where superscript 1 stands for the subdomain-1; the

subscripts 1, 2, 3 denote that the prescribed quantities are associated with the nodes in groups 1, 2, 3, respectively. The double subscript *ij*, *i*, *j*=1, 2, 3, is used to convey that the pair of nodes s_i and s_j in equations (8) and (9), by which the prescribed coefficient matrix blocks are computed, belong to group *i* and *j*, respectively.

Similarly, for subdomain-2 we have

$$\begin{bmatrix} U_{11}^2 & U_{12}^2 & U_{13}^2 \\ U_{21}^2 & U_{22}^2 & U_{23}^2 \\ U_{31}^2 & U_{32}^2 & U_{33}^2 \end{bmatrix} \begin{Bmatrix} x_1^2 \\ x_2^2 \\ x_3^2 \end{Bmatrix} = \begin{Bmatrix} H_1^2 \hat{\phi}_1^2 \\ H_2^2 \hat{\phi}_2^2 \\ H_3^2 \hat{\phi}_3^2 \end{Bmatrix} \tag{13}$$

$$\begin{bmatrix} Q_{11}^2 & Q_{12}^2 & Q_{13}^2 \\ Q_{21}^2 & Q_{22}^2 & Q_{23}^2 \\ Q_{31}^2 & Q_{32}^2 & Q_{33}^2 \end{bmatrix} \begin{Bmatrix} x_1^2 \\ x_2^2 \\ x_3^2 \end{Bmatrix} = \begin{Bmatrix} H_1^2 \hat{q}_1^2 \\ H_2^2 \hat{q}_2^2 \\ H_3^2 \hat{q}_3^2 \end{Bmatrix} \tag{14}$$

and for subdomain-3,

$$\begin{bmatrix} U_{11}^3 & U_{12}^3 & U_{13}^3 \\ U_{21}^3 & U_{22}^3 & U_{23}^3 \\ U_{31}^3 & U_{32}^3 & U_{33}^3 \end{bmatrix} \begin{Bmatrix} x_1^3 \\ x_2^3 \\ x_3^3 \end{Bmatrix} = \begin{Bmatrix} H_1^3 \hat{\phi}_1^3 \\ H_2^3 \hat{\phi}_2^3 \\ H_3^3 \hat{\phi}_3^3 \end{Bmatrix} \tag{15}$$

$$\begin{bmatrix} Q_{11}^3 & Q_{12}^3 & Q_{13}^3 \\ Q_{21}^3 & Q_{22}^3 & Q_{23}^3 \\ Q_{31}^3 & Q_{32}^3 & Q_{33}^3 \end{bmatrix} \begin{Bmatrix} x_1^3 \\ x_2^3 \\ x_3^3 \end{Bmatrix} = \begin{Bmatrix} H_1^3 \hat{q}_1^3 \\ H_2^3 \hat{q}_2^3 \\ H_3^3 \hat{q}_3^3 \end{Bmatrix} \tag{16}$$

At the interface between subdomain-*i* and *j*, both the temperature and heat flux must be continuous, i.e.,

$$\{\phi_i^j\} = \{\phi_j^i\} \tag{17}$$

$$\{q_i^j\} = -\{q_j^i\} \tag{18}$$

If we use the same set of nodes distributed on an interface in the discretization for both domains that share the interface, the following relationship exists:

$$\{H_i^j\} = \{H_j^i\} \tag{19}$$

Using the continuity conditions, equations (11)-(16) can be assembled into an overall matrix equation:

$$\begin{bmatrix} A_{11}^1 & A_{12}^1 & A_{13}^1 & 0 & 0 & 0 & 0 & 0 & 0 \\ U_{21}^1 & U_{22}^1 & U_{23}^1 & -U_{11}^2 & -U_{12}^2 & -U_{13}^2 & 0 & 0 & 0 \\ U_{31}^1 & U_{32}^1 & U_{33}^1 & 0 & 0 & 0 & -U_{11}^3 & -U_{12}^3 & -U_{13}^3 \\ Q_{21}^1 & Q_{22}^1 & Q_{23}^1 & Q_{11}^2 & Q_{12}^2 & Q_{13}^2 & 0 & 0 & 0 \\ 0 & 0 & 0 & A_{21}^2 & A_{22}^2 & A_{23}^2 & 0 & 0 & 0 \\ 0 & 0 & 0 & U_{31}^2 & U_{32}^2 & U_{33}^2 & -U_{21}^3 & -U_{22}^3 & -U_{23}^3 \\ Q_{31}^1 & Q_{32}^1 & Q_{33}^1 & 0 & 0 & 0 & Q_{11}^3 & Q_{12}^3 & Q_{13}^3 \\ 0 & 0 & 0 & Q_{31}^2 & Q_{32}^2 & Q_{33}^2 & Q_{21}^3 & Q_{22}^3 & Q_{23}^3 \\ 0 & 0 & 0 & 0 & 0 & 0 & A_{31}^3 & A_{32}^3 & A_{33}^3 \end{bmatrix} \begin{Bmatrix} x_1^1 \\ x_2^1 \\ x_3^1 \\ x_1^2 \\ x_2^2 \\ x_3^2 \\ x_1^3 \\ x_2^3 \\ x_3^3 \end{Bmatrix} = \begin{Bmatrix} d_1^1 \\ 0 \\ 0 \\ 0 \\ d_2^2 \\ 0 \\ 0 \\ 0 \\ d_3^3 \end{Bmatrix} \tag{20}$$

where $[A_{ij}^i]$ and $\{d_i^i\}$ are formed by merging $[U_{ij}^i]$ and $[Q_{ij}^i]$, $\{H_i^i \hat{\phi}_i^i\}$ and $\{H_i^i \hat{q}_i^i\}$, respectively, according to the known boundary conditions. For degrees of freedom with prescribed temperature, the related elements in $\{H_i^i \hat{\phi}_i^i\}$ are selected into $\{d_i^i\}$, and the corresponding rows of $[U_{ij}^i]$ are selected into $[A_{ij}^i]$; otherwise, elements in $\{H_i^i \hat{q}_i^i\}$ are selected into $\{d_i^i\}$, and the corresponding rows in $[Q_{ij}^i]$ are selected into $[A_{ij}^i]$.

The set of equation (20) is solved for the unknown parameters x, then, by back-substitution into equations (11)-(16), the boundary unknowns are obtained either on the interfaces or the external boundary surfaces.

The blocked matrix in equation (20) is actually hyper-matrix with smaller matrices as entries. The zero blocks in equation (20) give the equation a very beneficial characteristic, i.e. sparsity. To simply send the whole matrix to an equation-solving subroutine would be extremely inefficient. Techniques for banded or variable-banded matrix equation solving are also ineffective because of the lack of symmetry. To capitalize on the special structure of these sparse blocked matrices, we choose an iterative solver, i.e. GMRES, to solve it in this study. However, for the conventional GMRES, both the computational time and memory size required to store the coefficient matrix are proportional to n^2, where n is the total number of unknowns in the overall system of equations. This limits the method to relatively small scale problems. Accelerating the equation solution process with Fast Multipole techniques is necessary for solving large scale problems.

3. Accelerating multi-domain HdBNM with FMM

The FMM is called one of the top 10 algorithms of the 20th century. It is an algorithm for achieving fast products of particular dense matrices with vectors, and allows reduction of memory complexity in the methods based on Green's functions or fundamental solutions. The FMM uses multipole expansions (in term of series) to approximate the effects of a distant group of particles (nodes in HdBNM) on a local group, and thus achieves faster summation. Another aspect of FMM is that it uses a hierarchical decomposition of space to define ever-larger groups as distances increase. For 3D problems, an oct-tree decomposition is usually employed. We have implemented the FMM techniques in the HdBNM for single domain problems. In this paper, we will focus on how to accelerate the solution of equation (20).

When an iterative solver is employed to solve a linear system, the most time-consuming part of the solution process is the calculation of the matrix-vector product at each iteration step. Taking an iteration vector into account and considering equations (11)-(16), we suppose that

$$\begin{bmatrix} U_{11}^i & U_{12}^i & U_{13}^i \\ U_{21}^i & U_{22}^i & U_{23}^i \\ U_{31}^i & U_{32}^i & U_{33}^i \end{bmatrix} \begin{Bmatrix} x_1'^i \\ x_2'^i \\ x_3'^i \end{Bmatrix} = \begin{Bmatrix} \phi_1^i \\ \phi_2^i \\ \phi_3^i \end{Bmatrix} \tag{21}$$

and

$$\begin{bmatrix} Q_{11}^i & Q_{12}^i & Q_{13}^i \\ Q_{21}^i & Q_{22}^i & Q_{23}^i \\ Q_{31}^i & Q_{32}^i & Q_{33}^i \end{bmatrix} \begin{Bmatrix} x_1'^i \\ x_2'^i \\ x_3'^i \end{Bmatrix} = \begin{Bmatrix} q_1^i \\ q_2^i \\ q_3^i \end{Bmatrix} \tag{22}$$

where ϕ and q are result vectors of the products. Then, the

overall matrix-vector product in equation (20) can be obtained by

$$\begin{bmatrix} A_{11}^1 & A_{12}^1 & A_{13}^1 & 0 & 0 & 0 & 0 & 0 & 0 \\ U_{21}^1 & U_{22}^1 & U_{23}^1 & -U_{11}^2 & -U_{12}^2 & -U_{13}^2 & 0 & 0 & 0 \\ U_{31}^1 & U_{32}^1 & U_{33}^1 & 0 & 0 & 0 & -U_{11}^3 & -U_{12}^3 & -U_{13}^3 \\ Q_{21}^1 & Q_{22}^1 & Q_{23}^1 & Q_{11}^2 & Q_{12}^2 & Q_{13}^2 & 0 & 0 & 0 \\ 0 & 0 & 0 & A_{21}^2 & A_{22}^2 & A_{23}^2 & 0 & 0 & 0 \\ 0 & 0 & 0 & U_{31}^2 & U_{32}^2 & U_{33}^2 & -U_{21}^3 & -U_{22}^3 & -U_{23}^3 \\ Q_{31}^1 & Q_{32}^1 & Q_{33}^1 & 0 & 0 & 0 & Q_{11}^3 & Q_{12}^3 & Q_{13}^3 \\ 0 & 0 & 0 & Q_{31}^2 & Q_{32}^2 & Q_{33}^2 & Q_{21}^3 & Q_{22}^3 & Q_{23}^3 \\ 0 & 0 & 0 & 0 & 0 & 0 & A_{31}^3 & A_{32}^3 & A_{33}^3 \end{bmatrix} \begin{Bmatrix} x_1'^1 \\ x_2'^1 \\ x_3'^1 \\ x_1'^2 \\ x_2'^2 \\ x_3'^2 \\ x_1'^3 \\ x_2'^3 \\ x_3'^3 \end{Bmatrix} = \begin{Bmatrix} \phi_1^1 \text{ or } q_1^1 \\ \phi_2^1 - \phi_1^2 \\ \phi_3^1 - \phi_1^3 \\ q_2^1 + q_1^2 \\ \phi_2^2 \text{ or } q_2^2 \\ \phi_3^2 - \phi_2^3 \\ q_3^1 + q_1^3 \\ q_3^2 + q_2^3 \\ \phi_3^3 \text{ or } q_3^3 \end{Bmatrix} \tag{23}$$

The computational costs for the right hand side of equation (23) are trivial, and can be ignored. The summations in equations (21) and (22) can be accelerated by FMM within each single subdomain independently. In the above solution procedure, the coefficient matrix in equation (20) needs never be formed, and its use is purely symbolic. The matrix-vector product in equation (20) is divided into smaller scale ones at the subdomain level, thus making the fullest use of the sparsity pattern of the coefficient matrix, as consideration of the empty blocks is completely avoided.

The accelerated summation process by FMM for the sums in equations (21) and (22) is exactly the same as that in the FM-HdBNM for single domain problems. We create a hierarchical space decomposition tree for each subdomain. All the computer subroutines for single domain problems can be exploited here directly. We have described the algorithm of FM-HdBNM for single domain problems in references [6]. To avoid repetition, we will not discuss it here again. The reader is referred to the paper [6] for further details.

On the implementation of the above algorithm, we remark the following two aspects:

1. The sparsity pattern (population of the blocks) of the coefficient matrix in equation (20) has a severe impact on the condition number of the matrix, and thus on the solution procedure especially when an iterative equation solver is employed. The sparsity pattern of the system equation is determined by the ordering of unknowns. In order that the nonempty blocks in the overall system are as close to the main diagonal as possible, we use the particular ordering suggested by Kane [11]. The order is determined by listing all permutations of two subdomains as shown below:

$$11 \;\; 12 \;\; 13 \;\; 21^* \;\; 22 \;\; 23 \;\; 31^* \;\; 32^* \;\; 33$$

For permutations where the first digit is less than the second digit, blocks of potential are generated; otherwise, blocks of normal flux are generated. The permutations associated with blocks of normal flux are shown with an asterisk in the above list.

2. The selection of a good preconditioner for the GMRES is crucial for its convergence and computing efficiency. It is even more so with the multi-domain formulation, since the population of the overall equation matrix is no longer diagonally dominated. In this study as a primary step, we just simply use a block diagonal preconditioner that is obtained by inversing the diagonal blocked sub-matrices. These sub-matrices are the further smaller diagonal sub-blocks of the main diagonal blocked matrices, namely A_{11}^1, U_{22}^1, U_{33}^1, Q_{11}^2, A_{22}^2, U_{33}^2, Q_{11}^3, Q_{22}^3 and A_{33}^3, in equation (20). The sub-blocks are formed according to the leaves of the hierarchical decomposition tree. More precisely, if both the nodes $\mathbf{s}_I$ and $\mathbf{s}_J$ in equation (8) or (9) reside in the same leaf, the entry U_{IJ} or Q_{IJ} is selected into the corresponding sub-block. This preconditioner has been proposed by Nishida and Hayami [9] and adopted by Yoshida and Nishimura [10] for solving single-domain problems with FMM. This preconditioner may not be efficient for multi-domain problems. Developing other forms of preconditioners is an important subject of future research.

4. Test problems

The proposed techniques have been implemented in a code written in C++ and tested with two benchmark problems. All computations are carried out on the same desktop computer with an Intel(R) Pentium(R) 4 CPU (1.99GHz). Concerning the FMM and GMRES, we truncate all the infinite expansions after 10 terms, set the maximum number of boundary nodes in a leaf box to be 60, and terminate the iteration when the relative error is less than 10^{-6}. To assess the accuracy of the method, we calculate the relative error of nodal values of temperature using the following 'global' L_2 norm:

$$err = \frac{1}{|u|_{\max}} \sqrt{\frac{1}{n} \sum_{i=1}^{n} \left(u_i^{(e)} - u_i^{(n)} \right)^2} \tag{24}$$

where u_i represents nodal values of temperature ϕ or normal flux q, and $|u|_{\max}$ is the maximum value among the nodal values; n is the total number of nodes; the superscripts (e) and (n) refer to the exact and numerical solutions, respectively.

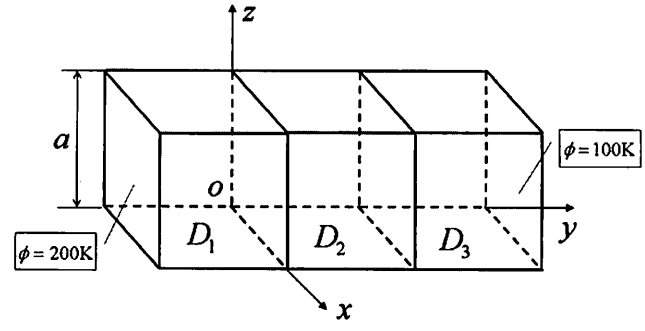

Figure 1. Geometry of the domain consisting of three cubes.

4.1 Three cubes with different material properties

A simple heat conduction problem is first considered. The domain of the problem consists of three equal cubes with different thermal conductivities (Figure 1). The side length of the cubes is $a = 1$ m. The used heat conductivities for cubes D_1, D_2 and D_3 are $\kappa_1 = 1.0$ W/mK, $\kappa_2 = 3.0$ W/mK and $\kappa_3 = 2.0$ W/mK, respectively. A uniform temperature of 200K is imposed at the left end face of cube D_1 and 100K at the right end face of cube D_3. All other outer surfaces are

prescribed as heat flux free. For this problem, the following exact solution is available:

$$\phi = \begin{cases} (1600\text{-}600\times y)/11, & -1 \le y < 0 \\ (1600\text{-}200\times y)/11, & 0 \le y < 1 \\ (1700\text{-}300\times y)/11, & 1 \le y \le 2 \end{cases} \quad (25)$$

We naturally treat each cube as a subdomain and perform computations on five node arrangements, namely, 10×10, 20×20, 40×40, 80×80 and 160×160 nodes uniformly distributed at each square surface of a subdomain. Results are summarized in Tables 1, in which the first and second columns list the number of nodes used on one square surface and the total number of nodes; the third and fourth columns list the number of iterations of GMRES and the total times for solving the system equations. In fifth and sixth columns, the relative errors of nodal values of temperature and normal flux are presented.

Table 1. Results for the domain consisting of three cubes

$k\times k$	*DOFs*	*Its*	T (s)	err_{temp}	err_{flux}
10×10	1800	18	313	1.2×10^{-5}	7.6×10^{-3}
20×20	7200	21	381	5.2×10^{-6}	3.6×10^{-3}
40×40	28800	24	2461	2.7×10^{-6}	1.8×10^{-3}
80×80	115200	32	13578	1.8×10^{-6}	1.3×10^{-3}
160×160	460800	44	72799	8.9×10^{-8}	1.2×10^{-4}

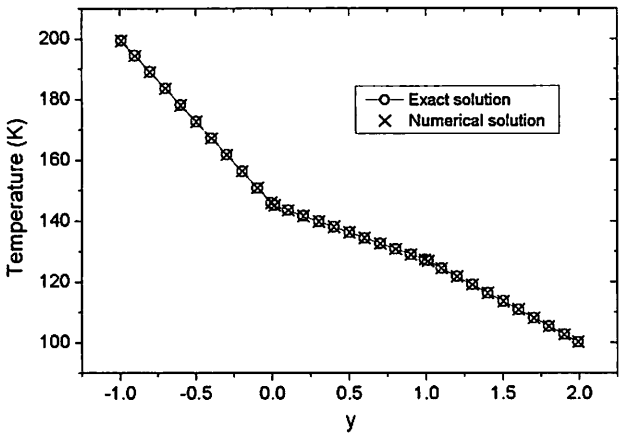

Figure 2. Temperature distribution along the central line.

Numerical results obtained for the temperature with 10×10 nodes on each square face, together with the exact solutions, along the central line from (0.5, -1.0, 0.5) to (0.5, 2.0, 0.5) are presented in Figure 2. The tabulated results show that our algorithm is capable of performing large-scale multi-domain computations. Highly accurate results are obtained with a small number of boundary nodes, and improved with increasing number of nodes used. The high accuracy is also demonstrated in Figure 2, where the numerical results agree excellently with the exact solution.

4.2 A cylinder of uniform material

The second example deals with a thick cylinder of uniform material (Figure 3). Dimensions are given as $a=5$, $b=7$ and $h=5$. We use this example to compare the efficiencies between the multi-domain and single domain solution strategies under the circumstance that FMM is employed to accelerate the equation solution. For this purpose, we first model the cylinder as a single domain (Figure 3a), and then decompose it into four subdomains (Figure 3b) and solve the problem by the multi-domain model. The following field distribution is used as the exact solution:

$$\phi = x^3 + y^3 + z^3 - 3yx^2 - 3xz^2 - 3zy^2 \quad (26)$$

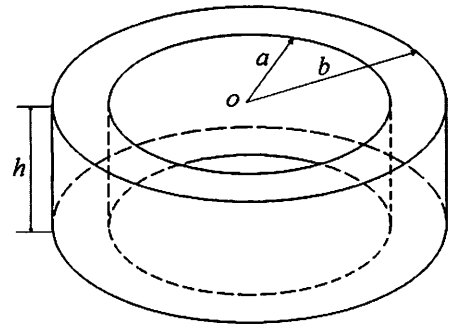

(a) Single domain model

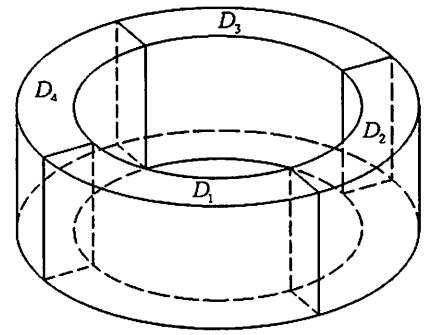

(b) Four subdomains model

Figure 3. Modeling of the hollow cylinder.

Potential boundary conditions are imposed on the inner and outer cylindrical surfaces and normal flux boundary conditions on the top and bottom faces, according to equation (26). Comparative computations are performed on five pairs of nodal arrangements for the two models. The total numbers of degrees of freedom for these nodal arrangements are listed in the first and fifth columns in Table 2 for the multi- and single-domain models, respectively. In each pair of nodal arrangements, for comparability, we discretize the outer surfaces in both models with the same set of nodes. Table 2 shows that the numbers of degrees of freedom for the multi-domain model are slightly bigger than the single-domain model. This difference is due to the additional unknowns that are introduced into the overall problem by the subdomain interfaces in the multi-domain model.

The second and sixth columns in Table 2 list the CPU seconds for computing the equation coefficients by the single- and multi-domain models, respectively. The third and seventh columns indicate the time used for solving the overall system of equations. In the fourth and eighth

columns, the relative errors of nodal values of potential are presented. It is seen that, in all cases of nodal arrangement, the single-domain model used slightly less CPU seconds both for computing coefficients and for solving equations than its multi-domain counterpart, while the results are equally accurate. This observation is in contrast to that made for the conventional multi-domain BEM [11], where both the accuracy and efficiency can be dramatically improved by the multi-domain techniques in modeling slender objects. The reason for this may be that, in the FMM context, only the coefficients for pairs of nodes in the near field are directly computed, and thus the required floating-point operation counts to build the coefficient matrix and to solve the equation are of order $O(n)$ rather than $O(n^2)$ in the conventional multi-domain BEM.

Table 2. Results for the thick cylinder problem

Multi-domain model			
DOFs	T_{coef} (s)	T_{equ} (s)	err_ϕ
11888	711	1167	5.1×10^{-4}
47448	4127	6418	1.6×10^{-4}
106688	7753	12516	9.9×10^{-5}
189608	22482	34743	7.1×10^{-5}
296208	33889	65317	4.1×10^{-5}
Single-domain model			
DOFs	T_{coef} (s)	T_{equ} (s)	err_ϕ
10288	530	803	5.7×10^{-4}
41048	3906	5203	1.6×10^{-4}
92288	8065	8937	9.5×10^{-5}
164008	20297	22378	6.8×10^{-5}
256208	33373	43899	5.4×10^{-5}

5. Conclusions

The FMM techniques have been implemented in a multi-domain formulation of the HdBNM for numerical solution of Laplace's equation. The matrix-vector multiplication during the equation solution process is split into smaller scale ones at the subdomain level, and is accelerated by the FMM independently within individual subdomains.

Two numerical examples are presented to study the performance of the proposed method. High accuracy and efficiency have been demonstrated. It is clear that the method is suitable for analyzing large-scale multi-domain problems such as modeling of composites. In the conventional BEM, multi-domain strategies are usually used to get better computational efficiency for long slender objects. For the multi-domain FM-HdBNM, however, this is no longer feasible, because the FMM has already reduced the computational scale to nearly linear complexity.

The block diagonal preconditioner based on the leaves in the FMM tree structure may not be efficient for multi-domain formulation, because the coefficient matrix in the multi-domain equation is no longer diagonally dominated. Developing other forms of preconditioner in the FMM context, such as the sparse approximate inverse preconditioner [13], is necessary for performing large-scale computations of practical interest. This is an important subject of future research.

Acknowledgements

This work was supported by the CLUSTER of Ministry of Education, Culture, Sports, Science and Technology, Japan.

References

1. Belytchko T, Lu YY, Gu L. Element free Galerkin methods. *Int. J. Num. Meth. Engng.*, Vol. 37 (1994), pp. 229-256.
2. Atluri SN, Zhu T. A new meshless local Petrov-Galerkin approach in computational mechanics. *Computational Mechanics*, Vol. 22 (1998), pp. 117-127.
3. Mukherjee YX, Mukherjee S. The boundary node method for potential problems. *Int. J. Num. Meth. Engng.*, Vol. 40 (1997), pp. 797-815.
4. Zhang JM, Yao ZH, Li H. A hybrid boundary node method. *Int. J. Num. Meth. Engng.*, Vol, 53 (2002), pp. 751-763.
5. Zhang JM, Tanaka M, Matsumoto T. Meshless analysis of potential problems in three dimensions with the hybrid boundary node method. *Int. J. Num. Meth. Engng.*, Vol. 59 (2004), pp. 1147-1160.
6. Zhang JM, Tanaka M, Endo M. The hybrid boundary node method accelerated by fast multipole method for 3D potential problems. *Int. J. Num. Meth. Engng.*, Vol. 63 (2005), pp. 660-680.
7. Rokhlin V. Rapid solution of integral equations of classical potential theory. *J. Comput. Phys.*, Vol. 60 (1985), pp. 187-207.
8. Greengard L, Rokhlin V. A new version of the Fast Multipole Method for the Laplace equation in three dimensions. *Acta Numerica*, Vol. 6 (1997), pp. 229-269.
9. Nishida, T., and Hayami, K., Application of the fast multipole method to the 3D BEM analysis of electron guns, In Marchettia, M., Brebbia, C.A., and Aliabadi, M.H., Eds., *Boundary Elements XIX*, Computational Mechanics Publications (1997), pp. 613–622.
10. Yoshida K, Nishimura N, Kobayashi S. Application of fast multipole Galerkin boundary integral equation method to elastostatic crack problems in 3D. *Int. J. Num. Meth. Engng.*, Vol. 50 (2001), pp. 525-547.
11. Kane JH. Boundary Element Analysis in Engineering Continuum Mechanics. Englewood Cliffs, NJ: Prentice-Hall, 1994.
12. Meric RA. Domain decomposition methods for Laplace's equation by the BEM. *Commun. Numer. Meth. Engng.*, Vol. 16 (2000), pp. 545-557.
13. Benzi M, Tuma M. A sparse approximate inverse preconditioner for nonsymmetric linear systems. *SIAM Journal on Scientific Computing*, Vol. 19 (1998), pp. 968-994.